Challenges in Panchromatic Modelling with Next Generation Facilities
Proceedings IAU Symposium No. 341, 2018
M. Boquien, E. Lusso, C. Gruppioni & P. Tissera, eds.

doi:10.1017/S1743921319004757

Panchromatic study of the first galaxies in cosmological simulations

Hidenobu Yajima[1], Shohei Arata[2], Makito Abe[1] and Kentaro Nagamine[2,3,4]

[1]Center for Computational Sciences, University of Tsukuba, 1-1-1 Tennodai, Tsukuba, Ibaraki 305-8577, Japan
email: yajima@ccs.tsukuba.ac.jp

[2]Department of Earth and Space Science, Graduate School of Science, Osaka University, Toyonaka, Osaka 560-0043, Japan

[3]Department of Physics & Astronomy, University of Nevada, Las Vegas, 4505 S. Maryland Pkwy, Las Vegas, NV 89154-4002, USA

[4]Kavli IPMU (WPI), The University of Tokyo, 5-1-5 Kashiwanoha, Kashiwa, Chiba, 277-8583, Japan

Abstract. Recent discoveries of high-redshift galaxies have revealed the diversity of their physical properties, from normal star-forming galaxies to starburst galaxies. To understand the properties of these observed galaxies, it is crucial to understand the star formation (SF) history, and the radiation properties associated with the SF activity. Here we present the results of cosmological hydrodynamic simulations with zoom-in initial conditions, and show the formation of the first galaxies and their evolution towards observable galaxies at $z = 6$. In addition, we show their multi-wavelength radiative properties. We find that star formation occurs intermittently due to supernova (SN) feedback at $z > 10$, and their radiation properties rapidly change with time. We suggest that the first galaxies are bright at UV wavelengths just after the starburst phase, and become extended Lyman-alpha sources. We also show that massive galaxies cause dusty starburst and become bright at infrared wavelengths.

Keywords. galaxies: formation, radiative transfer, methods: numerical

1. Introduction

Understanding galaxy formation is one of the main goals of today's astronomy. Recent observations have allowed us to detect distant galaxies in the early Universe (e.g., Finkelstein *et al.* 2013). The most distant galaxy confirmed by the observation of line emission has reached $z = 9.1$ (Hashimoto *et al.* 2018), and recent deep surveys are providing large samples of galaxies in the era of cosmic reionization at $z \gtrsim 6$ (e.g., Ouchi *et al.* 2018). In the next decade, the next generation telescopes, e.g., James Webb Space Telescope (JWST), Thirty Meter Telescope (TMT) and European Extremely Large Telescope (E-ELT) are going to study star formation in the first galaxies at $z \gtrsim 10$ focusing on UV continuum, Lyman-α line, and Hα line. Thus, it is vital to model the formation of galaxies in the current theoretical framework before the next generation telescopes will start to work. In addition, the first galaxies can be considered to be main ionizing sources for cosmic reionization (e.g., Yajima *et al.* 2011). Therefore, radiation properties of the first galaxies would also provide indispensable information for the cosmic reionization history.

2. Method

We use the smoothed particle hydrodynamics (SPH) code GADGET-3 (Springel 2005) with sub-grid models developed in the *First Billion Year* (FiBY) project (e.g., Khochfar & Dalla Vecchia *et al.* in prep.). We here use the star formation model based on the Kennicutt-Schmidt law (Schaye & Dalla Vecchia 2008), and the stochastic thermal feedback model for supernovae (Dalla Vecchia & Schaye 2012).

We make three zoom-in initial conditions that produce halos with $M_{\rm h} = 2.4 \times 10^{10}\,h^{-1}{\rm M}_{\odot}$ (Halo-10), $1.6 \times 10^{11}\,h^{-1}M_{\odot}$ (Halo-11) and $7.5 \times 10^{11}\,h^{-1}{\rm M}_{\odot}$ (Halo-12) at $z = 6$. The entire simulation box size is $(20\,h^{-1}{\rm Mpc})^3$ for Halo-10 and Halo-11, and $(100\,h^{-1}{\rm Mpc})^3$ for Halo-12 in a comoving units. In order to investigate the impacts of star formation and stellar feedback, using the initial condition of Halo-11, we also carry out other simulations with the lower star formation efficiency (Halo-11lowSF) and without stellar feedback (Halo-11noSN). In this work, we set the constant gravitational softening length of 200 h^{-1} pc in comoving scale and the minimum smoothing length of 20 h^{-1} pc.

As post-processing, we carry out the radiative transfer calculations for modeled galaxies by using the radiative transfer code, All-wavelength Radiative Transfer with Adaptive Refinement Tree (ART^2:Yajima *et al.* 2012). ART^2 is based on a Monte Carlo technique. We assume the Chabrier IMF with the mass range from 0.1 to 100 M$_{\odot}$. ART^2 uses an adaptive refinement grid structure. We set the maximum refinement level to 12 which achieves the resolution of 2.7 h^{-1}pc for Halo-11 at $z = 6$. First, we calculate the ionization structure of inter-stellar medium in galaxies. Then Lyα photon transfer is calculated with the emissivity based on the pre-calculated ionization structure. Finally we calculate the radiative transfer of stellar continuum and dust thermal emission. The dust temperature is estimated under the assumption of radiative equilibrium state. Thus our radiation transfer simulations show the multi-wavelength radiative properties of galaxies.

3. Results & Discussion

Figure 1 presents the maps of projected gas density for the Halo-11, Halo-11lowSF and Halo-11noSN at redshift $z = 7$. In the case of Halo-11 in our fiducial model, the gas structure shows highly inhomogeneous and clumpy features. No extended galactic gas disk is seen within the central ~ 2 kpc of Halo-11. On the other hand, disk-like structures are seen in Halo-11-noSN and Halo-11-lowSF models. This suggests the SF efficiency or the SN feedback have a large impact on the galactic morphology. The star formation is rather concentrated in the central nuclear region for the Halo-11-noSN, but the stellar distribution is more extended than the other runs due to larger amount of stars produced by $z = 7$. As a result, both SF efficiency and SN feedback affect the stellar distribution as shown in the lower panels of the figure.

Star formation histories are presented in Figure 2. At $z \gtrsim 10$, star formation is almost completely quenched due to stellar feedback after experiencing a star formation event with SFR ~ 0.1 M$_{\odot}$ s^{-1} in Halo-11. As the SFR decreases, SN feedback ceases to work. This allows the gas to fall down towards the galactic center, which leads to the next starburst. Repeating this cycle causes the oscillation of SFR. The peak and the minimum of SFR is different by a factor of $\gtrsim 2$ dex at $z \gtrsim 10$.

We find that a more massive halo (Halo-12) shows a rapid variation in SFR, similarly to Halo-11 at $z \gtrsim 10$. After the star formation at $z = 12.2$, the SN feedback evacuates the gas and quenches the star formation for a while until $z = 10.5$. As halos become more massive towards lower redshift, the deeper gravitational potential well can hold the

https://doi.org/10.1017/S1743921319004757 Published online by Cambridge University Press

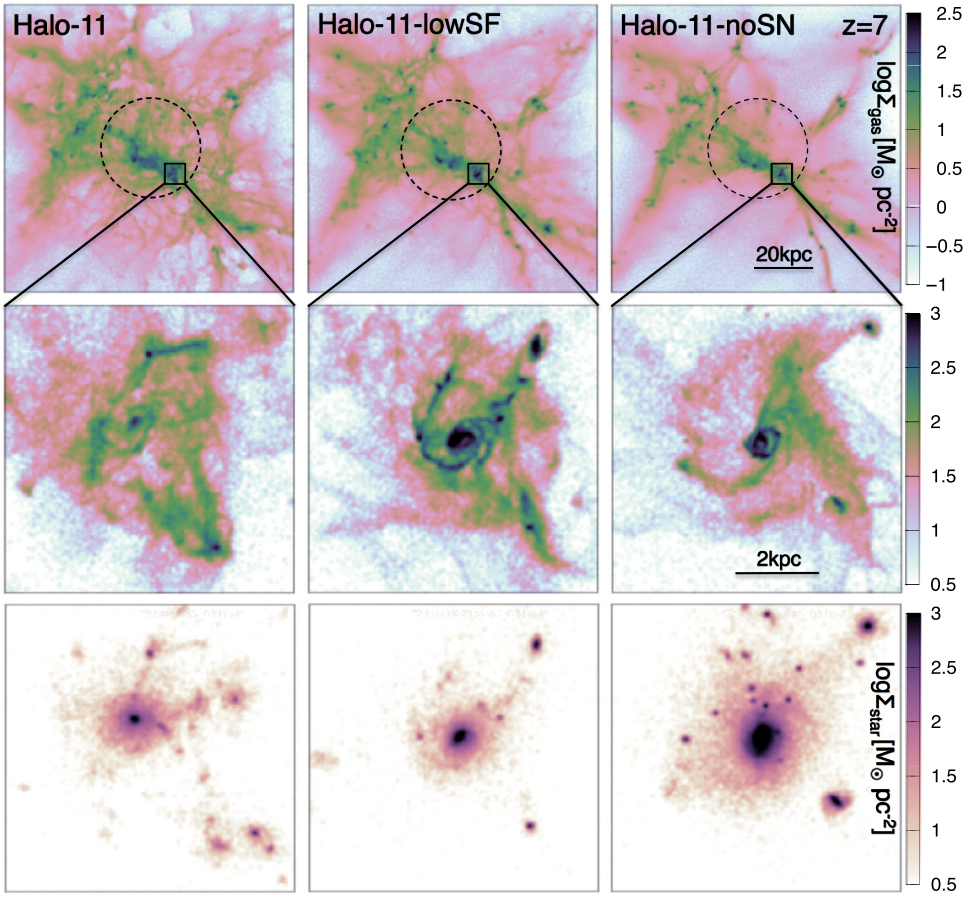

Figure 1. Column density of gas in Halo-11, Halo-11-lowSF, and Halo-11-noSN in units of $[M_\odot\,pc^{-2}]$ at $z=7$ (Figure 2 in Yajima *et al.* 2017). The top panels show the filamentary gas structure on a scale of physical 100 kpc, and the dashed circles show the virial radius of the most massive galaxy ≈ 18 kpc in the simulation boxes. The middle panels show the zoom-in view of the most massive galaxy in the halo with a scale of physical 7 kpc. The lower panels represent the stellar surface density with the same logarithmic scale as the middle panels.

gas against SN feedback, which allows for more continuous SF at $z \lesssim 10$. We find that Halo-11 and Halo-12 show similar SFRs as the observed LAEs at $z \sim 7$ and the SMG at $z = 7.5$ discovered by ALMA (Watson *et al.* 2015).

The escape fraction of UV continuum is shown in the second panel of Figure 2. At higher redshift $z > 10$, most of UV photons can escape because of low dust contents in galaxies. As the galaxy evolution proceeds, dusty gas covers star-forming regions and absorbs UV photons. The third and fourth panels show the fluxes at infrared and UV wavelengths in the rest frame. At lower redshifts, galaxies become bright at the infrared due to the dust absorption of UV photons. Our simulations show that ALMA would be able to detect the dust thermal emission from galaxies with the halo mass of $\gtrsim 10^{11}$ $M_\odot$ at $z \lesssim 9$. UV fluxes of galaxies increase with SFR as redshift decreases. We find that the bright wavelengths of galaxies rapidly change between UV and infrared due to the fluctuations of SFR and the escape fraction.

https://doi.org/10.1017/S1743921319004757 Published online by Cambridge University Press

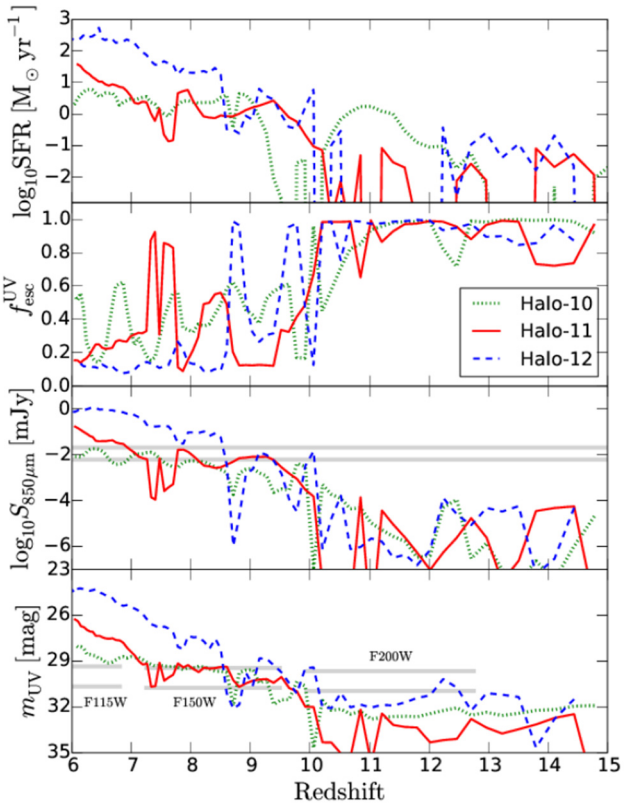

Figure 2. Redshift evolution of SFR (top panel), UV escape fraction (second panel), sub-mm flux (third panel) and emergent UV flux (bottom panel) are shown for Halo-10 (green dotted), Halo-11 (red solid), and Halo-12 (blue dashed). The gray horizontal lines in the third and forth panels show 3σ (lower line) and 10σ (higher line) detection thresholds for ALMA (full operation) and JWST with 10 hours time integration, which we obtained from the online calculators of each observatory.

Figure 3 represents the redshift evolution of Lyα luminosity ($L_{\rm Ly\alpha}$) and equivalent width (EW). We find that $L_{\rm Ly\alpha}$ fluctuates with the SF history. Halo-12 shows $L_{\rm Ly\alpha} \sim 10^{43}$ erg s^{-1} at $z \lesssim 7$, which reproduces observed bright LAEs (e.g., Finkelstein *et al.* 2013). Because of the lower SFR, $L_{\rm Ly\alpha}$ of Halo-11 is smaller than that of Halo-12 by a factor of ~ 10. At higher redshift $z \gtrsim 10$, the escape fraction of Lyα photons is almost unity because of the low dust contents in galaxies. Therefore, $L_{\rm Ly\alpha}$ depends on SFR and escape fraction of ionizing photons. At lower redshift $z < 10$, inter-stellar dust absorb Lyα photons. As SFR and the escape fraction fluctuate, EW also changes significantly. At the transition from star burst to quenched phases, EW increases rapidly. This is because galactic wind caused by supernovae allows Lyα photons to escape. At lower redshift $z \lesssim 8$, EW keeps low values of $\lesssim 40$ Å due to the large amounts of gas and dust.

Thus we show the multi-wavelength radiative properties of galaxies in the early Universe by combining cosmological hydrodynamics simulations and radiative transfer calculations. We find SFR and the radiative properties of the first galaxies rapidly change with time due to the stellar feedback. We show that massive galaxies with the halo masses of $\sim 10^{11} - 10^{12}$ M$_\odot$ reproduce observed galaxies successfully.

https://doi.org/10.1017/S1743921319004757 Published online by Cambridge University Press

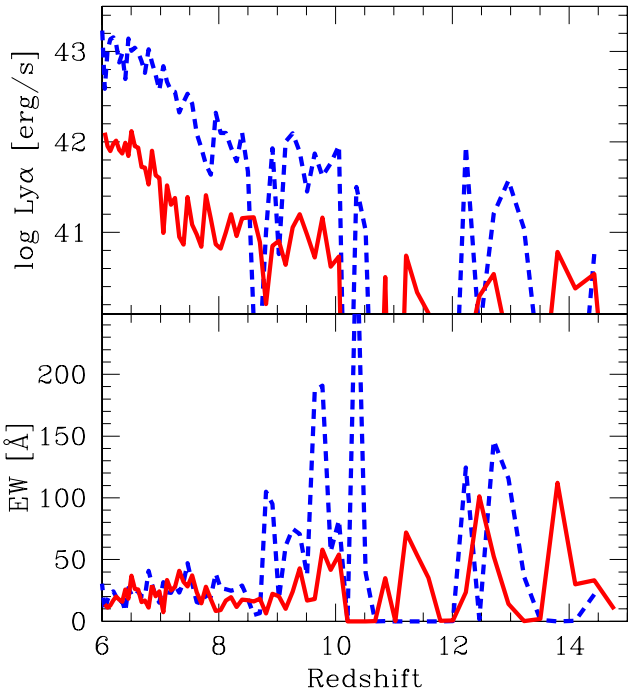

Figure 3. Redshift evolution of Lyα luminosity (upper panel) and equivalent width (lower panel). Red solid and blue dash lines show Halo-11 and Halo-12, respectively. The equivalent width is estimated by dividing the Lyα luminosity by UV luminosity density at 1300 Å in the rest frame.

References

Dalla Vecchia, C. & Schaye, J. 2012, *MNRAS*, 426, 140
Finkelstein, S. L., *et al.* 2013, *Nature*, 502, 524
Hashimoto, T. *et al.* 2018, *Nature*, 557, 392
Ouchi, M. *et al.* 2018, *PASJ*, 70, 13
Schaye, J. & Dalla Vecchia, C. 2008, *MNRAS*, 383, 1210
Springel, V. 2005, *MNRAS*, 364, 1105
Yajima, H., Choi, J. -H., & Nagamine, K. 2011, *MNRAS*, 412, 411
Yajima, H., Li, Y., Zhu, Q., & Abel, T. 2012, *MNRAS*, 424, 884
Yajima, H., Nagamine, K., Zhu, Q., Khochfar, S., & Dalla Vecchia, C. 2017, *ApJ*, 846, 30
Watson, D. *et al.* 2015, *Nature*, 519, 327

https://doi.org/10.1017/S1743921319004757 Published online by Cambridge University Press